

## Structures and magnetic properties of $\text{Pd}_n$ clusters ( $n = 3\text{--}19$ ) doped by Mn atoms

Yuewen Mu,<sup>1</sup> Yan Han,<sup>1</sup> Jinlan Wang,<sup>2</sup> Jian-guo Wan,<sup>1,\*</sup> and Guanghou Wang<sup>1</sup>

<sup>1</sup>National Laboratory of Solid State Microstructures, Department of Physics, Nanjing University, Nanjing 210093, People's Republic of China

<sup>2</sup>Department of Physics, Southeast University, Nanjing 210096, People's Republic of China

(Received 2 August 2011; published 2 November 2011)

The structures and magnetic properties of  $\text{Pd}_n$  and  $\text{Pd}_{n-1}\text{Mn}$  clusters ( $n = 3\text{--}19$ ) are investigated by using a spin-polarized density functional theory approach. Several different lowest-energy structures of  $\text{Pd}_n$  clusters ( $n = 11, 12, 14, 17$ ) are found. It is shown that when a Mn atom is doped into the  $\text{Pd}_n$  cluster, the cluster structure does not change for  $n < 9$ , while Mn doping gives rise to a geometry reconstruction for  $n > 9$ . The doping of a Mn atom enhances the stability of  $\text{Pd}_n$  clusters and increases their magnetic moment by a magnitude of  $(3\text{--}5)\mu_B$ . Moreover, we observe an evident oscillation of steplike magnetic behavior in  $\text{Pd}_n$  clusters upon doping of a Mn atom, and the origin of such a magnetic phenomenon is analyzed in detail.

DOI: 10.1103/PhysRevA.84.053201

PACS number(s): 36.40.Cg, 36.40.Mr, 61.46.Bc

### I. INTRODUCTION

The study of transition-metal clusters has been active for the past few decades due to their fundamental importance and potential applications. It is well known that palladium clusters are promising catalysts [1–3]. Recently, the observation of ferromagnetism in palladium clusters [4–6] made them potentially new magnetic storage materials [5]. Theoretical investigations revealed that small palladium clusters exhibit special magnetism in contrast to the nonmagnetic behavior of a single Pd atom and bulk Pd [7–9]. So the magnetic Pd clusters have drawn much attention in recent years, and much effort has been made in searching for stable Pd clusters with large magnetic moment.

In previous experimental investigations, some conflicting results on the magnetism of Pd clusters have been reported. Early Stern-Gerlach experimental measurements did not show magnetic moments in Pd clusters [10,11], whereas later photoelectron spectra of  $\text{Pd}_n^-$  clusters confirmed a magnetic behavior for  $\text{Pd}_n$  clusters when  $n < 15$  [4]. Subsequently, some groups also observed magnetic moments in a few topmost surface layers of Pd clusters with various sizes [5,6]. It is a pity that all these experiments did not provide sufficient information about the structural and electronic properties of Pd clusters, which is actually important for understanding their magnetic properties. Therefore, some theoretical investigations of Pd clusters were simultaneously carried out [7–9,12,13]. Among them, a representative work is the  $\text{Pd}_n$  clusters ( $n = 2\text{--}23, 55, 147$ ) reported by Kumar *et al.* [7]. They predicted an icosahedral growth pattern and size-dependent oscillatory magnetic moments which are not confined just to the surface atoms. Differently, Zhang *et al.* [9] recently found that the octahedral  $\text{Pd}_{19}$  cluster with fcc-like structures dominates the growth of  $\text{Pd}_n$  clusters ( $n = 15\text{--}25$ ), which tend to possess smaller magnetic moments than corresponding icosahedron-based structures.

Although many theoretical investigations have been done on palladium clusters, the ground-state structures for some sizes are still uncertain. Taking the  $\text{Pd}_{13}$  cluster as an example, earlier studies predicted the icosahedral structure as the ground

state [7,8], whereas a later study reported a buckled biplanar structure with lower energy [14]. However, very recently, a distorted hexagonal bilayerlike (HBL) structure was predicted to have lower energy than has ever been reported [15]. Therefore, in order to study the magnetism of palladium clusters and the size effect, a more refined search for the lowest-energy structures is required.

In addition, the magnetism modulation of palladium clusters is another important aspect for actual applications. Doping 3d transition-metal (TM) elements into a palladium cluster may be a valid avenue. It was reported that the fcc and bcc Pd bulk undergo a transition from paramagnetic ordering to ferromagnetic ordering when doped with Mn atoms, and the alloys become ferrimagnetic or antiferromagnetic with increasing Mn concentration [16]. A large magnetic moment in Mn substitution-doped  $\text{Pd}_{13}$  cluster was also predicted [17]. However, in current studies the magnetism evolution of the Mn-doped palladium clusters with their structure and size is seriously lacking, and how the Mn element influences the magnetic behavior of palladium clusters is still unclear.

In this work, we focus on the theoretical exploration of the structural and magnetic properties of  $\text{Pd}_n$  and bimetallic  $\text{Pd}_{n-1}\text{Mn}$  ( $n = 3\text{--}19$ ) clusters using a density functional theory method combined with a genetic algorithm and an embedded atom method. A more refined search for the lowest-energy structures of  $\text{Pd}_n$  clusters is performed and some additional cluster structures with lower energy are found. The evolution of the structural and magnetic properties of both  $\text{Pd}_n$  and  $\text{Pd}_{n-1}\text{Mn}$  clusters with size are studied. Our calculations show that the doping of a Mn atom not only enhances the stability of a  $\text{Pd}_n$  cluster but also generally increases its total magnetic moment by  $(3\text{--}5)\mu_B$ . Moreover, an evident oscillation of the steplike magnetic behavior is observed in the  $\text{Pd}_{n-1}\text{Mn}$  clusters, and the origin of such magnetic behavior is analyzed.

### II. COMPUTATIONAL METHODS

We perform a genetic algorithm [18] global search with an accurate embedded atom method (EAM) potential [19] to get the low-lying structures of  $\text{Pd}_n$  clusters ( $n = 8\text{--}19$ ). This EAM potential was parametrized based on an extensive set of density functional theory calculations of clusters and bulk; therefore, it is much better than early empirical potentials only

\*wanjg@nju.edu.cn

TABLE I. Comparison of our calculated binding energy per atom,  $E_b$  (eV), and bond length  $R_c$  (Å) with other theoretical results and experimental (Expt.) studies.

Species	Properties	Ours	Others	Expt.
Pd <sub>2</sub>	$E_b$	0.603	0.602 <sup>a</sup> (0.611 <sup>b</sup> )	0.698 <sup>c</sup>
	$R_c$	2.486	2.514 <sup>a</sup> (2.48 <sup>b</sup> )	2.48 <sup>c</sup>
Mn <sub>2</sub>	$E_b$	0.449	0.48 <sup>b</sup> (0.48 <sup>d</sup> )	(0.44 ± 0.30) <sup>d</sup>
	$R_c$	2.586	2.56 <sup>b</sup> (2.56 <sup>d</sup> )	3.17 <sup>e</sup>
PdMn	$E_b$	1.252		
	$R_c$	2.268		

<sup>a</sup>Reference [7].

<sup>b</sup>Reference [34].

<sup>c</sup>Reference [36].

<sup>d</sup>Reference [37].

<sup>e</sup>Reference [38].

fitted to bulk. The small Pd<sub>*n*</sub> clusters for  $n < 8$  have been extensively studied and no discrepancy was found in previous works [7,8,12,20,21]; therefore, a search of the low-lying structures of these clusters was not performed. A number of candidate structures (between 20 and 30) are obtained after 5000 mating steps. The child of each mating is optimized using the conjugate gradient method to achieve the maximum force threshold of 0.1 eV/Å.

Further geometry optimizations are carried out within the framework of spin-polarized density functional theory with the projector augmented wave (PAW) [22,23] pseudopotential method in the Vienna Ab Initio Simulation Package (VASP) [24,25]. The generalized gradient approximation with the Perdew-Burke-Ernzerhof (PBE) [26] exchange-correlation function is exploited. For a Pd atom,  $4p^6 4d^{10}$  electrons are treated as valance electrons while those of the Mn atom are  $3p^6 3d^5 4s^2$  electrons. A cubic supercell with a side dimension of 20 Å is employed, and only the  $\Gamma$ -point calculations are performed with a kinetic energy cutoff at 500 eV. The clusters are optimized using the conjugate gradient method without symmetry constraint until all the forces on each atom are less than 0.01 eV/Å. The accuracy of the present PBE-PAW scheme is assessed by benchmark calculations on Pd<sub>2</sub> and Mn<sub>2</sub> dimers. As shown in Table I, our results agree well with corresponding experimental values and previous theoretical results.

### III. RESULTS AND DISCUSSION

The low-lying structures of Pd<sub>*n*</sub> clusters ( $n = 8-19$ ) together with corresponding binding energy difference *between* the structure and the ground state, magnetic moments, and symmetries are presented in Fig. 1. In addition to the low-lying Pd<sub>*n*</sub> clusters reported before [7,9,12,13,27], several different ground-state structures, including Pd<sub>11</sub>, Pd<sub>12</sub>, Pd<sub>14</sub> and Pd<sub>17</sub> clusters, are found, which possess lower energy than ever reported at the PBE-PAW level. The ground-state geometries of Pd<sub>11</sub>, Pd<sub>12</sub>, and Pd<sub>14</sub> clusters resemble the ground-state structure of the Pd<sub>13</sub> cluster, which was regarded as a distorted HBL structure [15]. As for the ground-state geometry of Pd<sub>17</sub> (17a in Fig. 1), it is energetically preferred over the low-lying structure (17b in Fig. 1) by 6 meV, which was taken as the

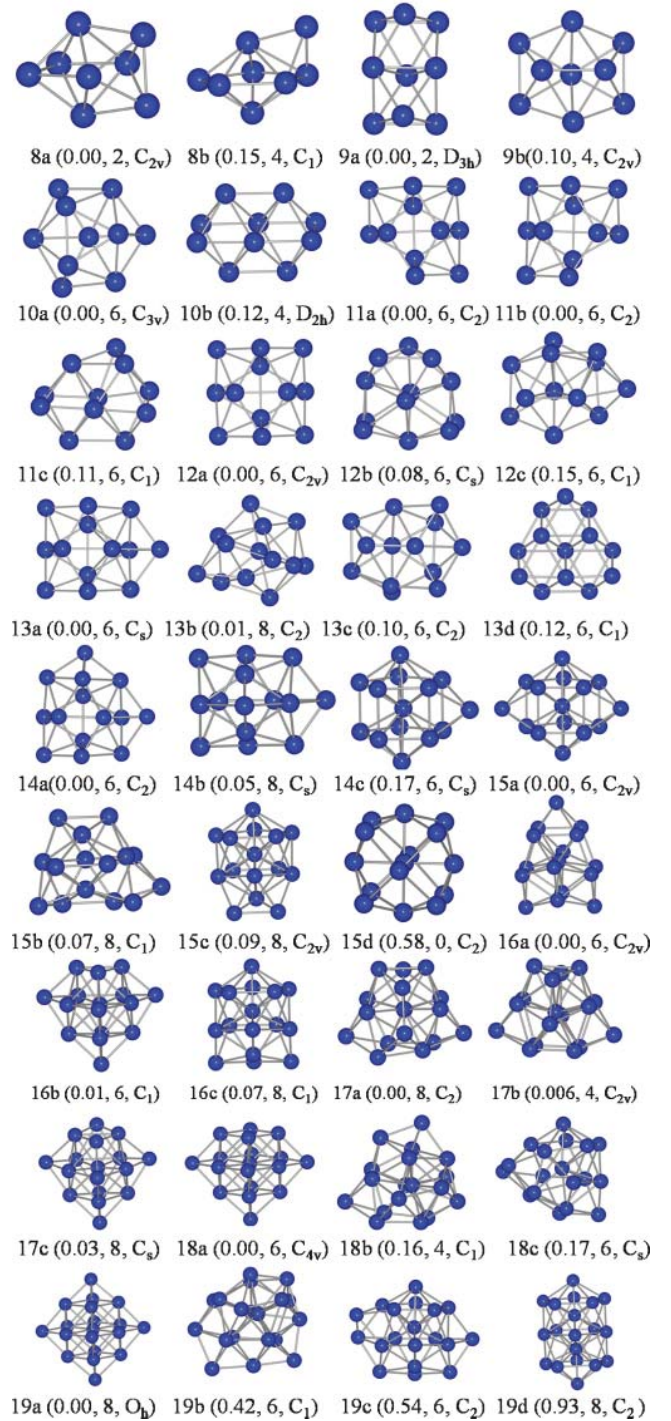


FIG. 1. (Color online) The low-lying structural isomers of Pd<sub>*n*</sub> clusters ( $n = 8-19$ ). The energy difference between isomers and corresponding ground state (eV), magnetic moment (units of  $\mu_B$ ), and symmetries are represented under every low-lying structure.

lowest-energy structure by Rogan *et al.* [13]. This energy discrepancy increases to 8 meV when the spin-orbit coupling (SOC) effect is taken into account, which is consistent with an early report that the SOC effect does not affect the relative stability of different structural isomers of Pd clusters [28]. In addition, our ground-state Pd<sub>17</sub> cluster can be regarded

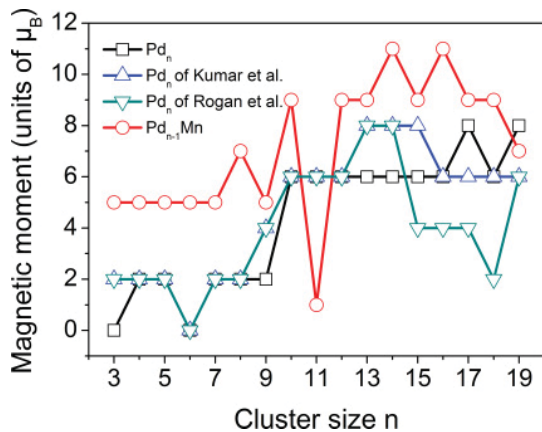


FIG. 2. (Color online) The total magnetic moments (units of  $\mu_B$ ) of Pd<sub>n</sub> and Pd<sub>n-1</sub>Mn clusters ( $n = 3-19$ ) and the magnetic moments of Pd<sub>n</sub> clusters obtained by Kumar *et al.* [7] and Rogan *et al.* [13].

as a distorted structure obtained by Rogan *et al.* due to the Jahn-Teller effect, further indicating that it is more stable. In addition, we notice that the symmetries of most of the low-lying structures obtained in the present work are lowered due to the Jahn-Teller effect.

The total magnetic moments of Pd<sub>n</sub> clusters as a function of cluster size  $n$  are plotted in Fig. 2. On the whole, the variation of the total magnetic moments of Pd<sub>n</sub> clusters with  $n$  shows a typical steplike behavior except for a trough at  $n = 6$ , and a magnetic moment jump occurs at  $n = 10$ . Comparing the magnetic moments of Pd<sub>n</sub> clusters obtained in the present work with those found earlier (also shown in Fig. 2), one notices that there exist significant deviations associated with conflicting trends of the magnetic moment with the cluster size. We consider that such deviations should be caused by the difference in lowest-energy structures since the magnetic energies are extremely sensitive to minute geometry changes [13]. In detail, the lowest-energy structures of Pd<sub>n</sub> clusters obtained by Kumar *et al.* are all icosahedral structures, which tend to possess larger magnetic moments due to their high symmetries and low mean coordination [7,29]. Differently, the lowest-energy structures of Pd<sub>n</sub> clusters obtained in the present work include various structures such as icosahedron-based, decahedron-based, fcc-like, and hexagonal bilayerlike structures. Although the variation trend of the magnetic moment with the cluster size is similar to that of Kumar *et al.*, the magnetic moments for some sizes (e.g.,  $n = 13, 14, 15$ ) are lower than those of Kumar *et al.*. On the other hand, the lowest-energy structures of Pd<sub>n</sub> clusters obtained by Rogan *et al.* also include various geometry structures. When  $n < 12$ , the variation trend of the magnetic moment with the cluster size is similar to Kumar *et al.*'s and ours; however, their magnetic moments for some sizes (e.g.,  $n = 15-18$ ) are much smaller than both Kumar *et al.*'s and ours. The main reason may be that their average bond lengths (2.64–2.65 Å) at these sizes are much smaller than Kumar *et al.*'s (2.70–2.75 Å) and ours (2.71–2.73 Å) [30,31].

Although similar magnetic step behavior of Pd<sub>n</sub> clusters was also reported by other groups [7,13], its origin is still unclear. To understand such a magnetic moment jump, we further calculate the  $s$ ,  $p$ , and  $d$  projected density of states

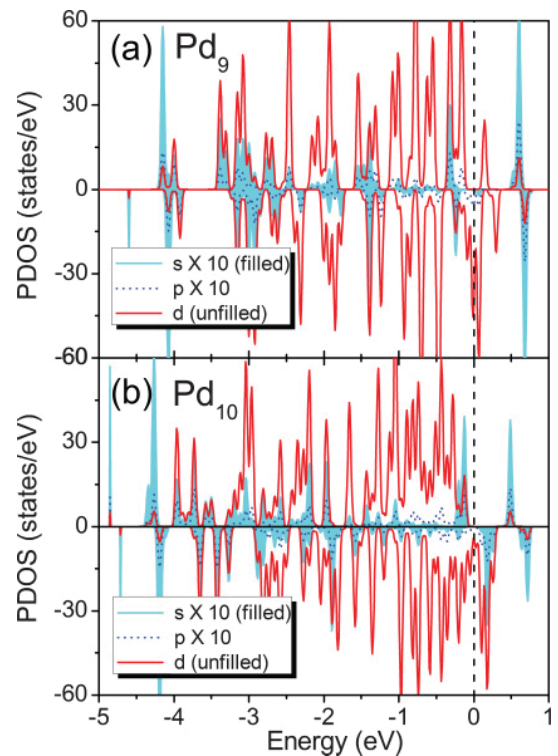


FIG. 3. (Color online) The  $s$ ,  $p$ , and  $d$  projected density of states (PDOS) of Pd<sub>9</sub> and Pd<sub>10</sub> clusters. The  $s$  and  $p$  PDOS are magnified 10 times so as to look into the  $spd$  hybridization. The filled-area (cyan) curve and unfilled-area (red) curve represent  $s$  and  $d$  PDOS, respectively. The black dashed line refers to the Fermi level, which is shifted to zero.

(PDOS) of the Pd<sub>9</sub> and Pd<sub>10</sub> clusters, as shown in Fig. 3. It is clearly seen that the magnetic moments of Pd<sub>n</sub> clusters mainly come from  $d$  states, while the  $s$  and  $p$  states only contribute a small amount of net spin. The hybridization between  $s$ ,  $p$ , and  $d$  states causes the closed-shell Pd atoms to have an incomplete  $d$ -shell configuration, which is usually responsible for the magnetism of TM clusters. We notice that, when the cluster size goes up from  $n = 9$  to  $n = 10$  where the magnetic step appears, the up- and down-spin subbands of the  $s$  and  $p$  states are split greatly, which consequently enhances significantly the depletion of down-spin  $4d$  states through  $spd$  hybridization and leads to a large magnetic moment of the Pd<sub>10</sub> cluster. We consider that the strong increase of the splitting between the spin-up and spin-down contributions of the  $s$  or  $p$  orbitals at  $n = 10$  is probably correlated with the abrupt increase of average bond length and average coordination number at this size (seen in Fig. 5), since the  $sd$  hybridization is very sensitive to the bond length [30].

To tune the magnetic properties of the Pd<sub>n</sub> cluster ( $n = 3-19$ ), we now attempt to dope a Mn atom into it to form a Pd<sub>n-1</sub>Mn cluster. Several low-lying structural isomers (between four and six) of Pd<sub>n</sub> clusters are chosen as the hosts for Mn doping. The optimized low-lying structures of Pd<sub>n-1</sub>Mn clusters ( $n = 3-19$ ) are presented in Fig. 4. It is seen that, for  $n = 3-9$ , the Mn substitution doping almost does not change the structure of the palladium clusters, and the lowest-energy structure of Pd<sub>n-1</sub>Mn is still similar to that of the corresponding



TABLE II. The average magnetic moment of Pd atom ( $M_1$ , units of  $\mu_B$ ) for Pd<sub>*n*</sub> clusters and the average magnetic moments of Pd atom ( $M_2$ , units of  $\mu_B$ ) and Mn atom ( $M_3$ , units of  $\mu_B$ ) for Pd<sub>*n-1*</sub>Mn clusters.

<i>n</i>	$M_1$	$M_2$	$M_3$	<i>n</i>	$M_1$	$M_2$	$M_3$
3	0.00	0.41	4.19	12	0.50	0.43	3.73
4	0.50	0.29	4.13	13	0.46	0.42	3.99
5	0.40	0.22	4.12	14	0.43	0.56	3.68
6	0.00	0.18	4.08	15	0.40	0.38	3.66
7	0.29	0.15	4.08	16	0.38	0.49	3.67
8	0.25	0.42	4.06	17	0.47	0.33	3.68
9	0.22	0.14	3.90	18	0.33	0.31	3.69
10	0.60	0.55	4.05	19	0.42	0.18	3.60
11	0.55	-0.27	3.53				

Pd and Mn, and (ii) much shorter length of the Pd-Mn bond [as seen in Fig. 5(c)], which causes a stronger Pd-Mn bond than the Pd-Pd bond (as seen in Table I).

The total magnetic moments of Pd<sub>*n-1*</sub>Mn clusters as a function of cluster size *n* are plotted in Fig. 2. After doping Mn, most of the palladium clusters have an enhanced total magnetic moment by (3–5) $\mu_B$ , and the average magnetic moment of Pd<sub>*n-1*</sub>Mn clusters increases to (0.37–1.67) $\mu_B$ , except for Pd<sub>10</sub>Mn. Table II lists the average magnetic moments of Pd and Mn atoms in Pd<sub>*n*</sub> and Pd<sub>*n-1*</sub>Mn clusters. It is seen that the magnetic moment of Mn atoms in Pd<sub>*n-1*</sub>Mn clusters is in the range (3.53–4.19) $\mu_B$  depending on the cluster size, which is much larger than that of Pd atoms in Pd<sub>*n-1*</sub>Mn clusters. This indicates that the increase of total magnetic moments of the clusters mainly comes from the doping Mn atom. Due to hybridization and interstitial contribution, the actual magnetic moment of Mn atoms in Pd<sub>*n-1*</sub>Mn clusters is smaller than expected by Hund's rules, but much larger than that of Mn<sub>*n*</sub> clusters with similar size, which is only in the range (0.4–1.7) $\mu_B$ /atom for *n* = 5–99 [32,33].

In addition, we find that the steplike magnetic behavior of Pd<sub>*n*</sub> clusters after doping Mn is disturbed, giving rise to an evident oscillation (as seen in Fig. 2). In detail, for some sizes (e.g., *n* = 8, 14, 16), the total magnetic moment of Pd<sub>*n*</sub> clusters is enhanced by 5 $\mu_B$  after doping, while for other sizes (e.g., *n* = 7, 9, 10, 12, 13, 15, 17, 18), the total magnetic moment only increases by 1 $\mu_B$  or 3 $\mu_B$ . Surprisingly, for *n* = 11 the total magnetic moment of Pd<sub>10</sub>Mn drops sharply to a very small value of 1 $\mu_B$ . From Table II we notice that such oscillating magnetic behavior is consistent with the variation of the average magnetic moment of Pd atoms, which is influenced by the doping Mn atom.

We now analyze the origin of such oscillating magnetic behavior. First, the Pd<sub>10</sub>Mn cluster is considered. From Table II and Fig. 5(c), we notice that, although the magnetic moment and average coordination number of Mn in the Pd<sub>10</sub>Mn cluster are similar to those of the clusters of neighboring size, the average Pd-Mn bond length of Pd<sub>10</sub>Mn is quite short, corresponding to a very small total magnetic moment. This implies that the magnetic moment of Pd<sub>*n-1*</sub>Mn clusters is very sensitive to the Pd-Mn bond length. In a previous investigation [34], Shen *et al.* also reported a similar computed result; i.e., shorter bond length could induce antiferromagnetic

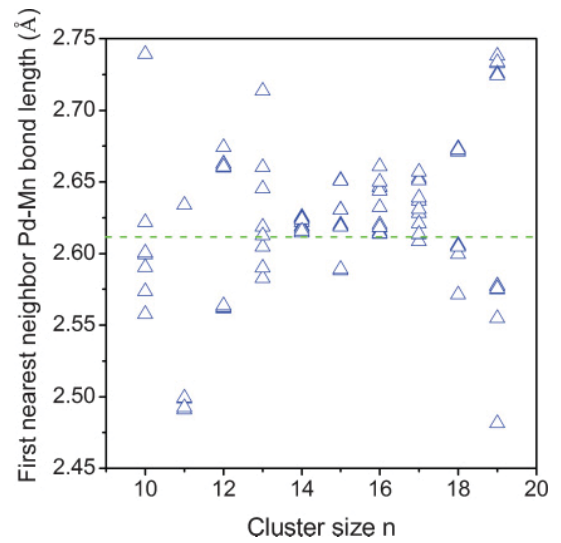


FIG. 6. (Color online) The distribution of Pd-Mn bond length between Mn and its nearest-neighbor Pd atoms in Pd<sub>*n-1*</sub>Mn clusters (*n* = 3–19).

coupling in Co<sub>*n-1*</sub>V (*n* = 2–9) clusters. Moreover, it was predicted that the fcc bulk Pd could undergo a transition from a nonmagnetic to a ferromagnetic state when the Pd-Pd bond length is elongated by about 5.5% [30,31]. That is to say, there exists a critical Pd-Pd bond length in bulk (about 2.90 Å) where the transition from a nonmagnetic to a ferromagnetic state occurs. Similarly, in our Pd<sub>*n-1*</sub>Mn clusters there may exist a critical Pd-Mn bond length where the magnetic moment varies greatly. Accordingly, we further plot the distribution of the Pd-Mn bond length between Mn and its nearest-neighbor Pd atoms in the Pd<sub>*n-1*</sub>Mn clusters with *n* > 9, as shown in Fig. 6. It is seen that the Pd-Mn bond length is distributed in a wide range of 2.48–2.74 Å. If we assume a critical Pd-Mn bond length of 2.61 Å, the evolution of the magnetism of the Pd<sub>*n-1*</sub>Mn clusters can be reasonably explained. For the Pd<sub>*n-1*</sub>Mn clusters with size *n* = 10, 12, 13, 15, 17, 18, since they all have several Pd-Mn bonds shorter than the critical bond length, the total magnetic moments are suppressed to a certain degree and only enhanced by 1 $\mu_B$  or 3 $\mu_B$ , in comparison with the pure Pd<sub>*n*</sub> clusters. However, for other size clusters (e.g., *n* = 14, 16), there is no Pd-Mn bond length shorter than the critical value, and thereby the total magnetic moments of the Pd<sub>*n-1*</sub>Mn cluster are enhanced significantly by up to 5 $\mu_B$  as compared with those of the Pd<sub>*n*</sub> clusters.

To gain more insight into the magnetism of the Pd<sub>*n-1*</sub>Mn clusters, it is essential to analyze the *s* and *d* PDOS of Pd<sub>*n-1*</sub>Mn clusters. The PDOS of *p* orbitals is not plotted because of its very small contribution. Here, we choose two clusters, i.e., Pd<sub>13</sub>Mn (*n* = 14) without Pd-Mn bonds shorter than the critical value and Pd<sub>14</sub>Mn (*n* = 15) with several Pd-Mn bonds shorter than the critical value, to make a comparison of their PDOS and magnetic structures, as shown in Fig. 7. It is seen that, similar to pure Pd<sub>*n*</sub> clusters, the *d* states of both Pd host atoms and doping Mn atoms in Pd<sub>*n-1*</sub>Mn clusters play a dominant role in the determination of total magnetic moment, whereas the contribution of *s* states is so small. For a Pd<sub>13</sub>Mn cluster, there is notable *sd* hybridization and large translation between

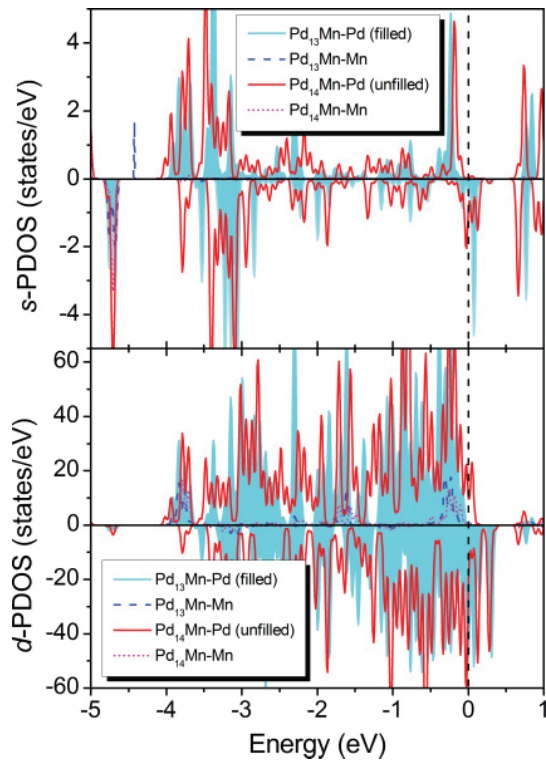


FIG. 7. (Color online) The  $s$  and  $d$  projected density of states (PDOS) of  $\text{Pd}_{13}\text{Mn}$  and  $\text{Pd}_{14}\text{Mn}$  clusters. The filled-area (cyan) line and unfilled-area (red) line represent PDOS of Pd atoms in  $\text{Pd}_{13}\text{Mn}$  and  $\text{Pd}_{14}\text{Mn}$  clusters, respectively. The black dashed line refers to the Fermi level, which is shifted to zero.

the spin-up and spin-down  $d$  PDOS, so a large magnetic moment arises. In contrast, for a  $\text{Pd}_{14}\text{Mn}$  cluster, due to shorter bonds, the strong interaction between the localized  $d$  states of Pd and Mn atoms pushes the spin-up  $d$  PDOS to higher levels, remarkably, while the spin-down  $d$  PDOS holds its position, consequently leading to smaller magnetic moment.

Finally, we turn to the  $\text{Pd}_{10}\text{Mn}$  cluster again and simply analyze its unique magnetic structure. Since there exist many very short Pd-Mn bonds in the  $\text{Pd}_{10}\text{Mn}$  cluster, much stronger  $d$ - $d$  interaction makes the number of spin-up electrons less than the number of spin-down electrons for Pd atoms. As a

consequence, the Mn atom tends to be antiferromagnetically coupled to Pd atoms (as seen in Table II) and further decreases the total magnetic moment. In brief, too-short bonds tend to cause strong  $d$ - $d$  interaction and small magnetic moment of the cluster. This is similar to the case of transition from ferromagnetic to antiferromagnetic ordering in the  $\text{Fe}_{13}$  cluster [35], in which antiferromagnetic order or admixtures of antiferromagnetic coordination appears when most of the bonds are short enough. In addition, it should be pointed out that only the  $\text{Pd}_{10}\text{Mn}$  cluster has the antiferromagnetic coordination in the size range of the present work. Such antiferromagnetic coordination may also appear for larger size  $\text{Pd}_{n-1}\text{Mn}$  clusters ( $n > 19$ ) if most of the Pd-Mn bonds are short enough. Further relative investigations are now under way.

#### IV. CONCLUSION

The geometries of both  $\text{Pd}_n$  and  $\text{Pd}_{n-1}\text{Mn}$  ( $n = 3-19$ ) clusters are calculated by using a spin-polarized density functional theory approach combined with a genetic algorithm and EAM. Several different lowest-energy structures of  $\text{Pd}_n$  clusters ( $n = 11, 12, 14, 17$ ) are found. For large cluster size ( $n > 9$ ), when a Mn atom is doped into the  $\text{Pd}_n$  cluster, it tends to occupy an interior site of the cluster and the geometry reconstruction generally occurs for the  $\text{Pd}_{n-1}\text{Mn}$  clusters. The doping of Mn atoms not only enhances the stability of  $\text{Pd}_n$  clusters but also increases their total magnetic moments by a magnitude of  $(3-5)\mu_B$ . Moreover, the doping of Mn atoms causes the  $\text{Pd}_{n-1}\text{Mn}$  clusters to give rise to an evident oscillation of steplike magnetic behavior, which is closely related to the Pd-Mn bond length and can be attributed to the  $d$ - $d$  interaction between Pd and Mn atoms.

#### ACKNOWLEDGMENTS

This work is supported by the National Key Projects for Basic Research of China (Grant No. 2010CB923401), the Provincial Nature Science Foundation of Jiangsu in China (Grant No. BK2008024), the PAPD project, and the National Natural Science Foundation of China (Grants No. 11134005 and No. 50972055). Our calculation is performed on a cluster system (consisting of eight LINKTEL-FX72 blade servers).

- [1] O. M. Wilson, M. R. Knecht, J. C. Garcia-Martinez, and R. M. Crooks, *J. Am. Chem. Soc.* **128**, 4510 (2006).
- [2] B. Kalita and R. C. Deka, *J. Am. Chem. Soc.* **131**, 13252 (2009).
- [3] A. S. Wörz, K. Judai, S. Abbet, and U. Heiz, *J. Am. Chem. Soc.* **125**, 7964 (2003).
- [4] G. Ganteför and W. Eberhardt, *Phys. Rev. Lett.* **76**, 4975 (1996).
- [5] T. Taniyama, E. Ohta, and T. Sato, *Europhys. Lett.* **38**, 195 (1997).
- [6] T. Shinohara, T. Sato, and T. Taniyama, *Phys. Rev. Lett.* **91**, 197201 (2003).
- [7] V. Kumar and Y. Kawazoe, *Phys. Rev. B* **66**, 144413 (2002).
- [8] M. Moseler, H. Häkkinen, R. N. Barnett, and U. Landman, *Phys. Rev. Lett.* **86**, 2545 (2001).
- [9] H. L. Zhang, D. X. Tian, and J. J. Zhao, *J. Chem. Phys.* **129**, 114302 (2008).
- [10] A. J. Cox, J. G. Louderback, S. E. Apsel, and L. A. Bloomfield, *Phys. Rev. B* **49**, 12295 (1994).
- [11] D. C. Douglass, J. P. Bucher, and L. A. Bloomfield, *Phys. Rev. B* **45**, 6341 (1992).
- [12] T. Futschek, M. Marsman, and J. Hafner, *J. Phys. Condens. Matter* **17**, 5927 (2005).
- [13] J. Rogan, G. García, M. Ramírez, V. Munoz, J. A. Valdivia, X. Andrade, R. Ramirez, and M. Kiwi, *Nanotechnology* **19**, 205701 (2008).
- [14] C. M. Chang and M. Y. Chou, *Phys. Rev. Lett.* **93**, 133401 (2004).

- [15] M. J. Piotrowski, P. Piquini, and J. L. F. Da Silva, *Phys. Rev. B* **81**, 155446 (2010).
- [16] C. Jing, Y. Yang, S. X. Cao, and J. C. Zhang, *Mod. Phys. Lett. B* **20**, 305 (2006).
- [17] S. Nigam, C. Majumder, and S. K. Kulshreshtha, *Phys. Rev. B* **76**, 195430 (2007).
- [18] D. M. Deaven and K. M. Ho, *Phys. Rev. Lett.* **75**, 288 (1995).
- [19] B. Shan, L. G. Wang, S. Yang, J. Hyun, N. Kapur, Y. J. Zhao, J. B. Nicholas, and K. Cho, *Phys. Rev. B* **80**, 035404 (2009).
- [20] W. Q. Zhang, Q. F. Ge, and L. C. Wang, *J. Chem. Phys.* **118**, 5793 (2003).
- [21] J. Rogan, G. Garcia, J. A. Valdivia, W. Orellana, A. H. Romero, R. Ramirez, and M. Kiwi, *Phys. Rev. B* **72**, 115421 (2005).
- [22] P. E. Blochl, *Phys. Rev. B* **50**, 17953 (1994).
- [23] G. Kresse and D. Joubert, *Phys. Rev. B* **59**, 1758 (1999).
- [24] G. Kresse and J. Furthmuller, *Phys. Rev. B* **54**, 11169 (1996).
- [25] G. Kresse and J. Hafner, *J. Phys.: Condens. Matter* **6**, 8245 (1994).
- [26] J. P. Perdew, K. Burke, and M. Ernzerhof, *Phys. Rev. Lett.* **77**, 3865 (1996).
- [27] F. Aguilera-Granja, A. Vega, J. Rogan, W. Orellana, and G. García, *Eur. Phys. J. D* **44**, 125 (2007).
- [28] P. Błoński and J. Hafner, *J. Phys. Condens. Matter* **23**, 136001 (2011).
- [29] V. Kumar and Y. Kawazoe, *Eur. Phys. J. D* **24**, 81 (2003).
- [30] H. Chen, N. E. Brener, and J. Callaway, *Phys. Rev. B* **40**, 1443 (1989).
- [31] L. Vitos, B. Johansson, and J. Kollár, *Phys. Rev. B* **62**, R11957 (2000).
- [32] M. B. Knickelbein, *Phys. Rev. Lett.* **86**, 5255 (2001).
- [33] M. B. Knickelbein, *Phys. Rev. B* **70**, 014424 (2004).
- [34] N. F. Shen, J. L. Wang, and L. Y. Zhu, *Chem. Phys. Lett.* **467**, 114 (2008).
- [35] P. Bobadova-Parvanova, K. A. Jackson, S. Srinivas, and M. Horoi, *Phys. Rev. B* **66**, 195402 (2002).
- [36] K. P. Huber and G. Herzberg, *Molecular Structure and Molecular Spectra IV. Constants of Diatomic Molecules* (Van Nostrand Reinhold, New York, 1979).
- [37] M. D. Morse, *Chem. Rev.* **86**, 1049 (1986).
- [38] K. D. Bier, T. L. Haslett, A. D. Kirkwood, and M. Moskovits, *J. Chem. Phys.* **89**, 6 (1988).